# Ecological function and exergy efficiency of Split-Heating Split-Expansion S-$CO_2$ Brayton cycle

Jianli Chen*, Qinglong Jin, Jialuo Huang

College of Power Engineering, Naval University of Engineering, Wuhan, Hubei, 430033, China

*Corresponding author's e-mail:M22380706@nue.edu.cn

**Abstract.** The Split-Heating Split-Expansion Supercritical $CO_2$ (S-$CO_2$) Brayton cycle finds application for the recovery of flue gas waste heat from gas turbines. In this paper, the Split-Heating Split-Expansion S-$CO_2$ Brayton cycle with finite temperature difference heat transfer, irreversible compression, irreversible expansion and other irreversible factors is studied. Subsequently, adopted the idea of finite time thermodynamics to study the cyclic ecological function and exergy efficiency under the conditions of mass flow rate, pressure ratio, shitter coefficient, current divider coefficient, distribution ratio of thermal conductivity, turbine efficiency and compressor efficiency changes. The results indicate that there is an optimal pressure ratio which maximizes the cyclic ecological function and exergy efficiency at different mass flow rates, compressor efficiencies, turbine efficiencies and discharge coefficients. The distribution ratio of thermal conductivity interacts to influence the cyclic ecological function and exergy efficiency.

**Keywords:** finite-time thermodynamics, Supercritical carbon dioxide Brayton cycle, Ecological function, Exergic efficiency.

## 1 Introduction

Currently, fossil fuel is heavily consumed in countries around the world, and problems such as energy crisis and environmental pollution are becoming increasingly serious [1]. With the enhancement of environmental protection awareness and the continuous growth of energy demand, the research and development of new and environmentally friendly energy conversion technology has become the common concern of all countries in the world. As part of its efforts to achieve carbon neutrality and carbon compliance, the Chinese government is proactively adjusting its industrial structure and developing new energy industry technologies [2-5]. Supercritical Carbon Dioxide (S-$CO_2$) can achieve supercritical status at room temperature because of its chemical properties, non-activity, non-flammable, safety, and low price [6]. Gas turbines, characterized by high efficiency, light weight and small size, are commonly used as driving engines for civil ships and warships. However, much energy is wasted due to the high waste heat temperature of the gas turbine flue gas, whereas the ideal

© The Author(s) 2024
A. E. Abomohra et al. (eds.), *Proceedings of the 2023 9th International Conference on Advances in Energy Resources and Environment Engineering (ICAESEE 2023)*, Atlantis Highlights in Engineering 29,
https://doi.org/10.2991/978-94-6463-415-0_71

heat source temperature of S-$CO_2$ matches the gas turbine exhaust temperature [7], making S-$CO_2$ promising in the field of gas turbine waste heat recovery [8-9].

The supercritical carbon dioxide Brayton cycle is of great potential to develop in new energy conversion system[10]. It can be applied to waste heat, renewable energy, and fossil fuels. Brayton cycle performance can be greatly enhanced by combining S-$CO_2$ with it. This combination also features such advantages as low operating noise, simplified design, compactness, and high system efficiency. Compared with the conventional steam Rankine cycle, the efficiency of S-$CO_2$ power cycle is noticeably higher. Yang et al. [11] calculated and examined the thermal efficiency of regenerative Brayton cycle and recompressed Brayton cycle; the findings of the study indicated that the inlet pressure and temperature of the compressor are the main factors in determining the thermal efficiency of the cycle. Matteo et al. [12] compared the current more advanced thermodynamic cycles, outlined the problems of the above cycles, and reviewed the research achievements of supercritical carbon dioxide cycles for three major applications, namely fuel cells, internal combustion engines and gas turbines. In this paper, Split-Heating Split-Expansion (SHSE) configuration was selected as the research object. The cycle aimed to improve the utilization rate of waste heat energy and reduce exergy loss in the heat exchanger. Finite time thermodynamics theory was adopted [13-16]. This is followed by analyses of exergy efficiency and cyclic ecological function were analyzed. Finite-time thermodynamics is a significant subfield of contemporary thermodynamic theory, which focuses on analysis and optimization under "finite time" or "finite scale" conditions. It realizes the fusion of numerous disciplines, including fluid mechanics, chemical reactions, heat transfer, and thermodynamics. In this paper, the performance of an irreversible SHSE S-$CO_2$ Brayton cycle, heat transfer between the accumulator and the working fluid, irreversible compression, irreversible expansion and other irreversible losses under a finite temperature difference were analyzed by applying the theory of finite time thermodynamics based on the literature [12].

## 2 Physical model of SHSE S-$CO_2$ Brayton cycle

Figure 1 and Figure 2 present the flow chart and *T-s* diagram of SHSE type S-$CO_2$ Brayton cycle device, respectively. The major components of the SHSE type S-$CO_2$ Brayton cycle include the compressor, heater, turbine, cooler, regenerator, and additional equipment.

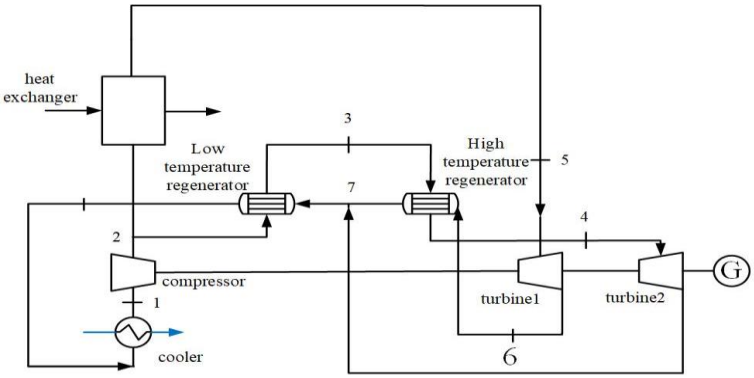


**Fig. 1.** Flow chart of SHSE S-$CO_2$ Brayton cycle device

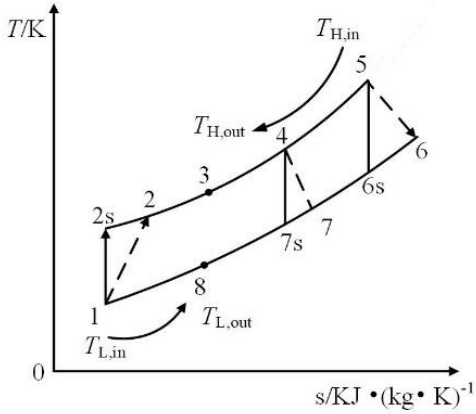


**Fig. 2.** T-s diagram of SHSE S-$CO_2$ Brayton cycle

In Figure 2, Process 1-2s is the ideal reversible adiabatic compression process in the compressor; Process 1-2 indicates the actual irreversible adiabatic compression process in the compressor, and the working medium is divided into 2 points.

The first working fluid:2-3-4-7. Process 2-3 is the isobaric heating process in the low temperature regenerator (the heat exchange is equivalent to Process 7-8). Process 3-4 is the constant pressure heating process in the high temperature regenerator (the heat exchange is equivalent to Process 6-7). Process 4-7 is the ideal reversible adiabatic expansion process in turbine 2, and Process 4-7 represents the actual irreversible adiabatic expansion process in turbine 2.

The second working medium 2:2-5-6-7. Process 2-5 is the isobaric heating process in the heat exchanger. Process 5-6s is an ideal reversible adiabatic expansion process in turbine 1. Process 5-6 represent the actual irreversible adiabatic expansion process in turbine 1. Process 6-7 is the isobaric cooling process in the high-temperature regenerator (the heat exchange is equal to the 3-4 process).

The two streams converge at point 7 in the diagram. Process 7-8 is the isobaric cooling process in the low temperature regenerator (the heat exchange is equivalent to Process 2-3). The Process 8-1 is the isobaric cooling process in the cooler.

Define the ratio as the shunt coefficient, then there is the following formula:

$$m_{wf,1}=x_p \cdot m_{wf} \tag{1}$$

$$m_{wf,2}=(1-x_p) \cdot m_{wf} \tag{2}$$

The efficiency of the compressor can be expressed as follows:

$$\eta_p=(h_{2,s}-h_1)/(h_2-h_1) \tag{3}$$

Where $\eta_p$ is the isentropic efficiency of the compressor.

The efficiency of the turbine can be expressed as follows:

$$\eta_{t1}=(h_5-h_6)/(h_5-h_{6,s}) \tag{4}$$

$$\eta_{t2}=(h_4-h_7)/(h_4-h_{7,s}) \tag{5}$$

Where $\eta_{t1}$ is the isentropic efficiency of turbine 1, and $\eta_{t2}$ is the isentropic efficiency of turbine 2.

Cycle heat absorption rate:

$$Q_H=U_H \frac{[(T_{H,in}-T_5)-(T_{H,out}-T_2)]}{\ln[(T_{H,in}-T_5)/(T_{H,out}-T_2)]}=c_{pH} \cdot m_H \cdot (T_{H,out}-T_{H,in})=x_p \cdot m_{wf} \cdot (h_5-h_2) \tag{6}$$

Where $Q_H$ is the total heat absorption in the heat exchanger during the process of 2-5, $U_H$ is the thermal conductivity in the heat exchanger, $T_{H,in}$ is the inlet temperature of the heat exchanger, $T_{H,out}$ is the outlet temperature of the heat exchanger. $c_{pH}$ is the isobaric specific heat of the heat exchanger, in unit $\mathrm{kJ \cdot (kg \cdot K)^{-1}}$. $m_H$ is the mass flow rate of the heat exchanger, and the unit is $\mathrm{kg \cdot s^{-1}}$. $x_p$ is the split ratio of 2-5-7. $m_{wf}$ is the mass flow rate of the working medium, and the unit is $\mathrm{kg \cdot s^{-1}}$.

rate of heat release:

$$Q_L=U_L \frac{[(T_8-T_{L,out})-(T_1-T_{L,in})]}{\ln[(T_8-T_{L,out})/(T_1-T_{L,in})]}=c_{pL} \cdot m_L \cdot (T_{L,out}-T_{L,in})=m_{wf} \cdot (h_8-h_1) \tag{7}$$

Where $Q_L$ is the heat discharge in the cooler, $U_L$ is the thermal conductivity in the cooler. $T_{L,in}$ and $T_{L,out}$ are the inlet temperature and outlet temperature of the cooler respectively. $c_{pL}$ is the isobaric specific heat of the cooler in unit $\mathrm{kJ \cdot (kg \cdot K)^{-1}}$. $m_L$ denotes the mass flow rate of the cooler, expressed in $\mathrm{kg \cdot s^{-1}}$.

regeneration rate:

$$Q_{R1}=U_{R1} \frac{[(T_6-T_4)-(T_7-T_3)]}{\ln[(T_6-T_4)/(T_7-T_3)]}=x_p \cdot m_{wf} \cdot (h_6-h_7)=(1-x_p) \cdot m_{wf} \cdot (h_6-h_7) \tag{8}$$

$$Q_{R2}=U_{R2} \frac{[(T_7-T_3)-(T_8-T_2)]}{\ln[(T_7-T_3)/(T_8-T_2)]}=m_{wf} \cdot (h_7-h_8)=(1-x_p) \cdot m_{wf} \cdot (h_3-h_2) \tag{9}$$

Where $Q_{R1}$ and $Q_{R2}$ are the heat transfer in the high temperature regenerator and the low temperature regenerator respectively, $U_{R1}$ and $U_{R2}$ signify the thermal conductivity in the high temperature regenerator and the low temperature regenerator respectively.

$$U_T=U_H+U_L+U_{R1}+U_{R2} \tag{10}$$

Where $U_T$ is the total thermal conductivity.

The net power can be expressed as follows:

$$W_{net}=x_p \cdot m_{wf} \cdot (h_5-h_6)+(1-x_p) \cdot m_{wf} \cdot (h_4-h_7) - m_{wf} \cdot (h_2-h_1) \tag{11}$$

The ecological function is used as a thermodynamic performance index to characterize the trade-off between the cyclic output power and the entropy production rate, which is modified by Yan Zijun [17]. The cyclic entropy production rate and ecological function E could be seen as follows:

$$S_g=m_L \cdot c_{pL} \cdot \ln\left(\frac{T_{L,out}}{T_{L,in}}\right)-m_H \cdot c_{pH} \cdot \ln\left(\frac{T_{H,in}}{T_{H,out}}\right) \tag{12}$$

$$E=W_{net}-T_0 S_g \tag{13}$$

And the exergy efficiency could be defined as:

$$\eta_{ex}=W_{net}/e_H \tag{14}$$

In this paper, a finite time force thermodynamic analysis and optimization program for the new supercritical carbon dioxide cycle was written by MATLAB software. Using the given boundary conditions ($T_{H,in}$ , $T_{L,in}$ , $U_H$ , $U_{R1}$ , $U_{R2}$ , $U_L$ ,$\eta_{t1}$ ,$\eta_{t2}$ ,$\eta_p$), a fsolve function was applied to solve the temperature and specific enthalpy at each state point, and then the cycle performance was calculated based on the specific enthalpy.

## 3 Numerical examples and discussion

One of the main applications of the model is the waste heat recovery of LM-2500PE G4 gas turbine. According to literature [18], the heat source is set to be the high temperature flue gas emitted by gas turbines ($N_2$:78.12%, $O_2$:20.96%, Ar: 0.92%), and the cold source is cold water. Using REFPROP in MATLAB, one can determine the specific heat capacity of both the heat source and the cold supply at constant pressure. Table 1 displays the initial design point parameters.

**Table 1.** Initial design parameters

| Parameter | Symbol | Value |
|---|---|---|
| Heat source inlet temperature | $T_{H,in}$ | 805.15 K |
| Cold source inlet temperature | $T_{L,in}$ | 298.15 K |
| Mass flow rate of flue gas | $m_H$ | 89.9 kg·s$^{-1}$ |
| Cooling water mass flow rate | $m_L$ | 1 000 kg·s$^{-1}$ |
| Mass flow rate of working medium | $m_{wf}$ | 120 kg·s$^{-1}$ |
| current divider coefficient | $x_p$ | 0.6 |
| Minimum circulating pressure | $p_{min}$ | 7.7 MPa |
| Maximum circulating pressure | $p_{max}$ | 20 MPa |
| Turbine 1 efficiency | $\eta_{t1}$ | 0.89 |
| Turbine 2 efficiency | $\eta_{t2}$ | 0.89 |
| Compressor efficiency | $\eta_P$ | 0.89 |
| Thermal conductivity of high temperature regenerator | $U_{R1}$ | 1050 kW·K$^{-1}$ |
| Thermal conductivity of heater | $U_H$ | 450 kW·K$^{-1}$ |
| Thermal conductivity of low temperature regenerator | $U_{R2}$ | 750 kW·K$^{-1}$ |
| Thermal conductivity of cooler | $U_L$ | 750 kW·K$^{-1}$ |
| Cooling water specific heat capacity at constant pressure | $c_{p,L}$ | 4 181.3 kJ·(kg·K)$^{-1}$ |
| Specific heat capacity of flue gas at constant pressure | $c_{p,H}$ | 1 103.7 kJ·(kg·K)$^{-1}$ |

The relationship between the cyclic $E$ and the pressure ratio ($\pi$) is presented in Figure 3 for a shunt coefficient of 0.5 and a mass flow rate $m_{wf}$ in the range of 80kg·s$^{-1}$-110kg·s$^{-1}$. For each given $m_{wf}$, there is an optimal $\pi$ that maximizes $E$, and the $E$ decreases as the $\pi$ increases. This is because $\pi$, as an important index affecting the cycle performance, directly or indirectly affects the size of $E$, and changes with the change of $m_{wf}$, and it also contributes to specifying the $E$ value. In practical engineering applications, an appropriate $\pi$ can be selected to achieve the optimal value of $E$.

Figure 4 shows the change of $\eta_{ex}$ with $\pi$ when the shunt coefficient is 0.5 and the mass flow rate $m_{wf}$ is in the range of 80kg·s$^{-1}$-110kg·s$^{-1}$. As can be seen in the figure, the cyclic $\eta_{ex}$ versus $\pi$ does not vary linearly with $m_{wf}$. For each given $m_{wf}$, there is an optimal $\pi$ to maximize $\eta_{ex}$, and the maximum value of $\eta_{ex}$ decreases with the increase of $m_{wf}$. When $\pi$ is small, $\eta_{ex}$ increases with the increase of $m_{wf}$ and when π is large, $\eta_{ex}$ decreases with increasing $m_{wf}$.

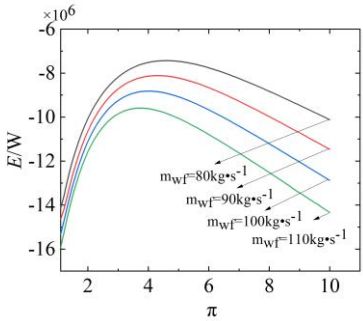


**Fig. 3.** Effect of $m_{wf}$ on $E$-$\pi$ relation

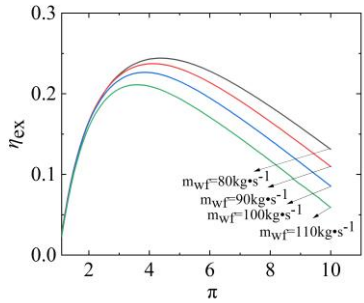


**Fig. 4.** Effect of $m_{wf}$ on $\eta_{ex}$-$\pi$ relation

The relationship between cycle $E$ and π for compressor and turbine efficiencies in the 0.8-1.0 range is graphically illustrated in Figure 5. Under the same π, $E$ gradually increases with the increase of $\eta_{t1}$, $\eta_{t2}$ and $\eta_p$. Figure 6 shows the change of exergy with $\pi$ when the shunt coefficient is 0.4 and $\eta_{t1}$, $\eta_{t2}$, and $\eta_p$ are in the range of 0.8-1.0. Under the same $\pi$, with the increase of $\eta_{t1}$, $\eta_{t2}$ and $\eta_p$, $\eta_{ex}$ gradually increases. This is because $\eta_{t1}$, $\eta_{t2}$ and $\eta_p$ reflect the irreversibility inside the turbine in the cycle, and the larger the $\eta_{t1}$, $\eta_{t2}$ and $\eta_p$, the lower the irreversibility of the turbine and compressor, the less energy loss, the greater the $E$; for each given $\eta_{t1}$, $\eta_{t2}$, and $\eta_p$, there is a critical $\pi$ that maximizes $\eta_{ex}$.

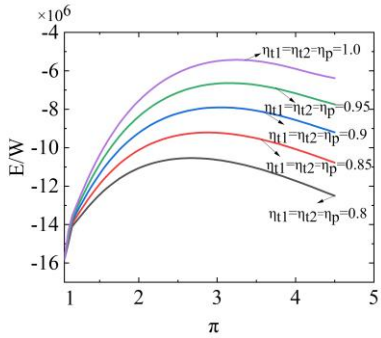


**Fig. 5.** Effect of $\eta_p$, $\eta_{t1}$, $\eta_{t2}$ on $E$-$\pi$ relation

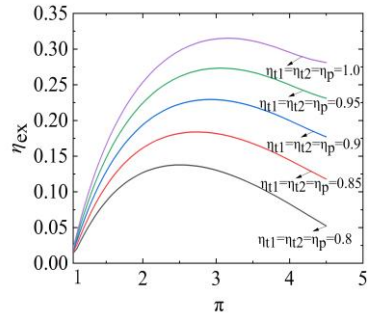


**Fig. 6.** Effect of $\eta_p$, $\eta_{t1}$, $\eta_{t2}$ on $\eta_{ex}$-$\pi$ relation

The 3D plot of the variation of cyclic $E$ with $m_{wf}$ in the range of 0.35-0.60 $m_{wf}$ is presented in Figure 7. It can be seen from the figure that when the $m_{wf}$ is a constant value, the cyclic $E$ gradually decreases with the increase of the $x_p$. When the diversion coefficient is constant, $E$ decreases with the increase of $m_{wf}$. Figure 8 shows a three-dimensional diagram of $\eta_{ex}$ changing with mass flow rate in the range of 0.4-0.6. When the mass flow rate was constant, the $\eta_{ex}$ increases with decreasing shunt coefficient.

The effect of varying the circulation shunt coefficient on $E$ for $\pi$ between 1 and 6 is demonstrated in Figure 9. It can be seen from the figure that for a certain mass flow

rate, there exists an optimal $\pi$ that maximises $E$. $\pi$ is the characteristic parameter corresponding to the operation of the device, and the interaction of the shunt coefficient affects the cycle performance.

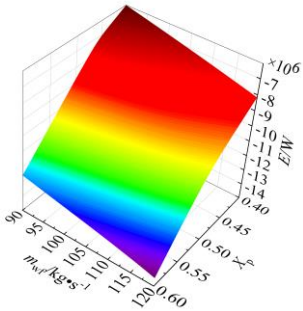


**Fig. 7.** Effect of $x_p$on $E$--$m_{wf}$ relation

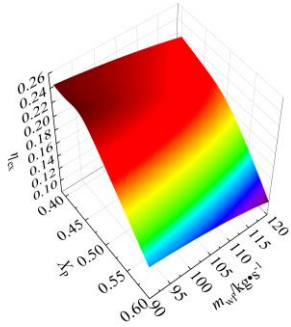


**Fig. 8.** Effect of $x_p$on $\eta_{ex}$-$m_{wf}$ relation

Figure 10 reveals the influence of $\eta_{ex}$ with the change of circulation shunt coefficient in the range of $\pi$ ranges from 1 to 6. As can be seen from the figure, $\eta_{ex}$ shows a three-dimensional parabolic shape, and when $\pi$ is fixed, there is an optimal shillage coefficient that leads to the optimal value of $\eta_{ex}$.

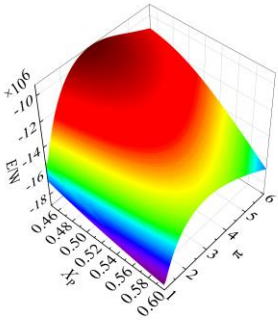


**Fig. 9.** Effect of $x_p$ on $E$—$\pi$ relation

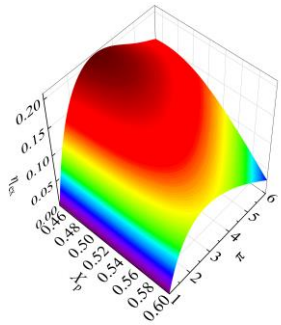


**Fig. 10.** Effect of $x_p$ on $\eta_{ex}$—$\pi$ relation

Figure 11 exhibits the effect of changes in the high-temperature regenerator and heater on $E$. The figure illustrates that when the thermal conductivity distribution ratio of the heater is kept constant, $E$ tends to increase and then decrease as the thermal conductivity distribution ratio of the high temperature regenerator grows. Figure 12 shows the impact of $\eta_{ex}$ of high-temperature regenerator and heater in the range of 0.1-0.45. It can be seen that $\eta_{ex}$ first increased and then decreased with the increase of thermal conductivity of heater and thermal conductivity distribution ratio of high-temperature regenerator.

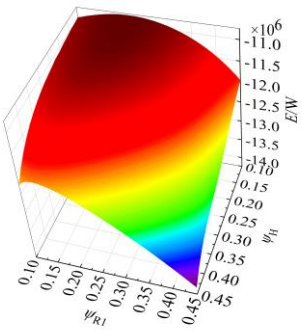


**Fig. 11.** Effect of $\psi_H$ on $E$—$\psi_{R1}$ relation

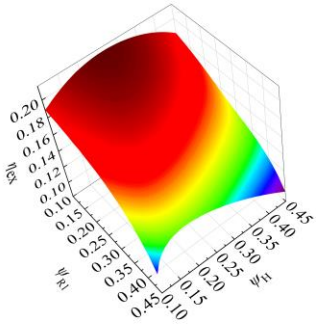


**Fig. 12.** Effect of $\psi_H$ on $\eta_{ex}$—$\psi_{R1}$ relation

## 4 Conclusion

In this paper, an irreversible SHSE type supercritical carbon dioxide Brayton dynamic cycle model is established under the condition of variable temperature heat source by using the finite time thermodynamics theory. The influences of $m_{wf}$, $x_p$, $\pi$, $\eta_{t1}$, $\eta_{t2}$ and $\eta_p$ on $E$ and $\eta_{ex}$ are analyzed and the results can be seen as follows:

1. For different $m_{wf}$, $x_p$, $\pi$, $\eta_{t1}$, $\eta_{t2}$ and $\eta_p$, there exists an optimal $\pi$, that can maximize the cyclic $E$ and $\eta_{ex}$.

2. When the shitter coefficient is small, the $\pi$ and $m_{wf}$ can be increased to increase the cyclic $E$ and $\eta_{ex}$. When the thermal conductivity distribution of the high temperature regenerator is relatively small, $E$ and $\eta_{ex}$ can be improved by increasing the thermal conductivity distribution ratio of heater.

From the analysis, it can be concluded that each parameter in the cycle contributes to the cyclic interactions and the cyclic performance can be improved by subsequent optimization.

## References

1. Xu M, Lin B, Wang S.: Towards energy conservation by improving energy efficiency? Evidence from China's metallurgical industry [J]. Energy 216, 119255 (2021).
2. Padilla R V, Too Y C S, Benito R, et al: Exergetic analysis of supercritical $CO_2$ Brayton cycles integrated with solar central receivers [J]. Applied Energy 148, 348-365(2015).
3. Østergaard P A, Duic N, Noorollahi Y, et al.: Sustainable development using renewable energy technology [J]. Renewable energy 146, 2430-2437 (2020).
4. Schulze M, Nehler H, Ottosson M, et al.: Energy management in industry–a systematic review of previous findings and an integrative conceptual framework [J]. Journal of cleaner production 112, 3692-3708(2016).
5. LI Q, NIU J, WANG Q.: Research on the Construction of New Energy Automotive Industry Innovation System based on Low-carbon Economy [J]. ENERGY 1(2), 85-90 (2011).

6. Liu Y, Wang Y, Huang D.: Supercritical $CO_2$ Brayton cycle: A state-of-the-art review [J]. Energy 189, 115900 (2019).
7. Wang W, Chen L, Sun F.: Ecological optimisation of an irreversible-closed ICR gas turbine cycle [J]. International Journal of Exergy 9(1), 66-79 (2011).
8. Sharan P, Neises T, McTigue J D, et al.: Cogeneration using multi-effect distillation and a solar-powered supercritical carbon dioxide Brayton cycle[J]. Desalination 459, 20-33 (2019).
9. Tao Z, Zhao Q, Tang H, et al.: Thermodynamic and exergetic analysis of supercritical carbon dioxide Brayton cycle system applied to industrial waste heat recovery [J]. Proc. CSEE 39, 6944-6951 (2019).
10. Khatoon S, Kim M H. Preliminary design and assessment of concentrated solar power plant using supercritical carbon dioxide Brayton cycles[J]. Energy Conversion and Management 252, 115066(2022).
11. Wang X, Li X, Li Q, et al. Performance of a solar thermal power plant with direct air-cooled supercritical carbon dioxide Brayton cycle under off-design conditions[J]. Applied Energy 261, 114359(2020).
12. Xia S J, Jin Q L, Wu Z X.: Exergy Efficiency Analyses and Optimization of Regenerative S-$CO_2$ Brayton Cycle[J]. Journal of South China University of Technology(Natural Science Edition) 50(2), 111-120 (2022).
13. Wu F, Chen L G, Sun F R, et al.: Finite-time exergoeconomic performance bound for a quantum Stirling engine [J]. International journal of engineering science 38(2) ,239-247(2000).
14. Liu X W, Chen L G, Wu F, et al.: Ecological optimization of an irreversible harmonic oscillators Carnot heat engine [J]. Science in China Series G: Physics, Mechanics and Astronomy 52(12), 1976-1988 (2009).
15. Ge Y L, Chen L G, Sun F R. Finite time thermodynamic modeling and analysis for an irreversible Atkinson cycle [J]. Thermal Science 14(4), 887-896 (2010).
16. Feng H, Chen L, Sun F. Optimal ratios of the piston speeds for a finite speed irreversible Carnot heat engine cycle [J]. International Journal of Sustainable Energy 30(6), 321-335 (2011).
17. Yan Z: Comment on “An ecological optimization criterion for finite-time heat engines”[J. Appl. Phys. 69, 7465 (1991)] [J]. Journal of Applied Physics 73(7), 3583(1993).
18. Na S I, Kim M S, Baik Y J, et al.: Optimal allocation of heat exchangers in a Supercritical carbon dioxide power cycle for waste heat recovery [J]. Energy Conversion and Management 199: 112002(2019).

**Open Access** This chapter is licensed under the terms of the Creative Commons Attribution-NonCommercial 4.0 International License (http://creativecommons.org/licenses/by-nc/4.0/), which permits any noncommercial use, sharing, adaptation, distribution and reproduction in any medium or format, as long as you give appropriate credit to the original author(s) and the source, provide a link to the Creative Commons license and indicate if changes were made.

The images or other third party material in this chapter are included in the chapter's Creative Commons license, unless indicated otherwise in a credit line to the material. If material is not included in the chapter's Creative Commons license and your intended use is not permitted by statutory regulation or exceeds the permitted use, you will need to obtain permission directly from the copyright holder.